Injection-locked Oscillator Coupled to Two External Resonators for Wireless Power Transfer

Franco Ramírez, Almudena Suárez

Universidad de Cantabria, Spain
{ramirezf, almudena.suarez}@unican.es

***Abstract* —We present a near-field wireless power transfer system based on an injection-locked oscillator coupled to two external resonators, one used as a relay element. We demonstrate that injection locking mitigates the instability problems observed in free-running conditions and provides a more regular behavior versus the coupling conditions. The system is investigated with a semi-analytical formulation based on a nonlinear oscillator model extracted from harmonic balance (HB) in the presence of the input source. This model is combined with the input admittance of the coupled network, accounting for the two external resonators. We analyze the output power of the locked solution and its dependencies on the coupling factors and load resistance. A versatile design methodology is derived, which is validated with full HB simulations and measurements.**

***Keywords* — Oscillator, injection locking, WPT**

I. Introduction

Near-field wireless power transfer, achieved through inductive coupling between two resonators, finds practical applications in recharging electric vehicles, sensor networks, and biomedical implants [1]-[2]. However, the efficiency of the power transfer diminishes with the distance and misalignment between the coils, due to the associated reduction of the coupling factor. The use of an intermediate (relay) resonator proves beneficial in overcoming obstacles or achieving extended distances [3]-[4]. To excite this coupled system, an independent source, followed by a driver and a power amplifier, is typically used. Alternatively, a free-running oscillator can be employed, which integrates the three functions in a single circuit. Besides a more compact implementation, the oscillator-based system will typically reduce the total power consumption, as demonstrated in [5]. A drawback is the variation of the oscillation frequency with the coupling conditions [6], which may lead the system to operate out of the allowed frequency bands. When using a relay resonator, the resulting additional resonances may also give rise to undesired oscillation modes, as shown in [7]. These undesired modes can be eliminated with the aid of a trap resonator [7], but a careful tuning is required to avoid the reduction of the transfer efficiency.

As an alternative solution, here we will investigate the injection locking of the oscillator coupled to two external resonators, one of them acting as a relay element. Note that injection locking had been previously considered in the single resonator system of [8] to prevent the variation of the oscillation frequency. Instead, here we deal with two external resonators, both having an impact on the locked operation. By means of a harmonic-balance (HB) method [8], we will initially demonstrate that injection locking mitigates the instability problems and gives rise to a more regular behavior. An in-depth investigation of the locked operation will also be carried out through a semi-analytical formulation based on a realistic oscillator model. This will provide insight into the dependence of the locked solution on the coupling factors and the load resistance. It will also enable the derivation of a versatile design methodology, which will be validated with full HB simulations and measurements.

II. Injection Locked Operation

We will consider the system shown in Fig. 1, in which a Class-E oscillator is coupled to a relay resonator (L_2, C_2) that is, in turn, coupled to a receiver resonator (L_3, C_3). Note that, as demonstrated in [9], the coupling between the coils L_1 and L_3 can be neglected when the distance between them is relatively larger than their radii. The oscillator is expected to operate at 13.56 MHz. For comparison, we will initially suppress the input source ($E_g = 0$), that is, we will consider the system in free-running conditions [7]. Fig. 2(a) shows the variation of the oscillation power and frequency versus the coupling factor k_1 when $k_2 = 0.25$. Note that k_1 is limited to $k_1 = 0.3$ since we target operation at relatively long distances. Besides the variation of the oscillation frequency, the system exhibits two oscillation modes. Mode 1 is the one corresponding to the core oscillation, since it starts from $k_1 = 0$, (uncoupled conditions). However, it is extinguished at a relatively low k_1, whereas an undesired mode (Mode 2) arises at $k_1 = 0.29$. In [9], the above problems were circumvented using a trap. Here we will introduce a locking source with amplitude E_g at the frequency ω.

For the analysis of the injection-locked oscillator, we will apply the method in [8], briefly summarized for completeness. We introduce a current-type auxiliary generator (AG) at ω[Fig. 1(b)], connected in series at the gate port. This AG is used to calculate the oscillator impedance function Z_{AG} as the ratio between the AG voltage and current. This is combined with Thevenin's equivalent of the input network, obtained through the linear analysis of the input network [Fig. 1(b)]. The aim is to obtain the function F_{th} that relates Thevenin's voltage V_{th} to E_g. Assuming periodic behavior at the frequency ω, we have the following outer-tier system:

$$\begin{aligned} &Z_{AG}(I_{AG},\omega,k_1,k_2)I_{AG} = V_{th} \quad \text{(a)} \\ &V_{th} = F_{th}(\omega)E_g \quad \text{(b)} \end{aligned} \quad . \tag{1}$$

Note that Z_{AG} in (1)(a), obtained with HB, is nonlinear, whereas (1)(b) is nonlinear. Combining the two equations, we get:

$$\left| Z_{AG}(I_{AG},\omega,k_1,k_2) / F_{th}(\omega) \right| I_{AG} = E_g \, . \tag{2}$$

Initially, we will perform an analysis versus E_g at the frequency $f=\omega/(2\pi)$ =13.56 MHz under k_1 = 0.1 and k_2 = 0.25. For a direct comparison with the free-running behavior [Fig. 2(a)] no retuning for the oscillator core or external resonators is carried out. To obtain the periodic solution curve versus E_g, we sweep I_{AG} and calculate E_g through (2). The output power P_{out} is traced in blue in Fig. 2(b). It is multivalued with two turning points: T_1 and T_2. The results obtained with (2) have been validated with default HB, which jumps from the lower to the upper section. For E_g below T_2 the system is unlocked and exhibits an undesired quasi-periodic solution (not represented). The oscillation gets locked at T_2 and the upper section of the multivalued curve is the only stable one. This is verified with pole-zero identification [9] in Fig. 2(c), which shows the variation of the real part of the dominant poles versus E_g when $\omega/(2\pi)$ =13.56 MHz. The point T_2 is obtained at a lower E_g as ω approaches the free-running frequency. See the curve corresponding to f=13.88 MHz, traced in red in Fig. 2(b). Thus, high output power can be obtained with much lower input level than in the case of a power amplifier.

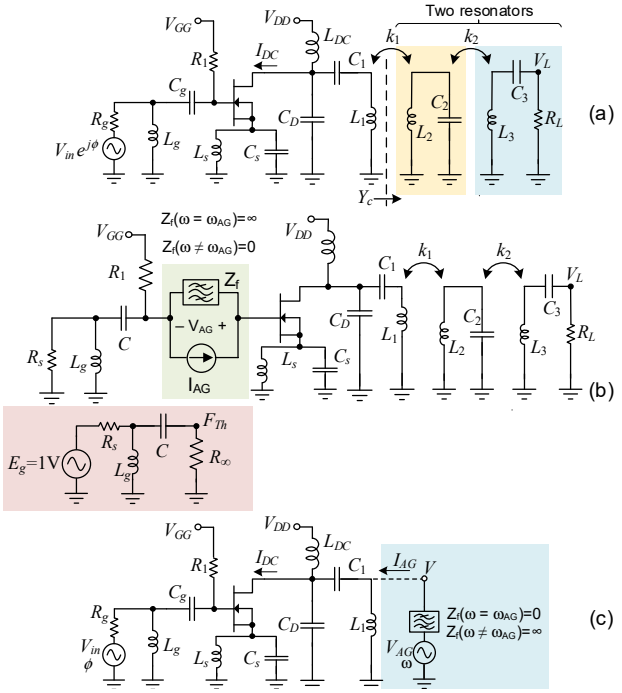

Fig. 1. Injection-locked oscillator coupled to two external-resonators. (a) Schematic. (b) Setup for the full HB analysis (2). The oscillator is simulated in the absence of the input source, using a current AG to obtain $Z_{AG}(I_{AG},\omega,k_1,k_2)$. The input network (with E_g = 1 V) is analyzed to calculate F_{th}. (c) Setup to extract the admittance function $Y(V,\phi,\omega)$ considered in (3).

To obtain the solution curves versus any of the two coupling factors (k_1 or k_2) for a given ω and E_{go}, we perform a double sweep in k_1 or k_2 and the AG current I_{AG}, and we trace the constant amplitude contour (2) (with $E_g = E_{go}$) in the plane defined by I_{AG} and k_1 or k_2. The output power and drain efficiency are calculated through interpolation of V_L and I_{DC} [Fig. 2(a)]. Fig. 2(d) shows the solution curve versus k_1 for k_2 = 0.25, at f = 13.56 MHz and E_g = 0.63 V. For the lower k_1 we obtain the same three sections observed in Fig. 2(b). The upper section is the only stable one. In comparison with the free-running case [Fig. 2(a)], a more regular behavior is obtained, with no variation of the oscillation frequency.

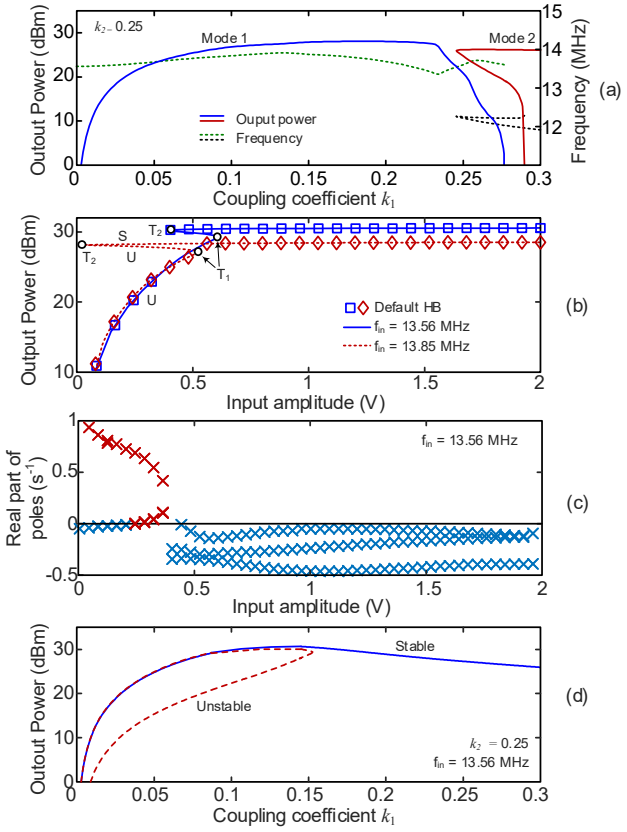

Fig. 2. (a) Free-running solution versus k_1 for k_2 = 0.25 [9], used as a reference. (b) Injection-locked curve versus E_g for k_1 = 0.1 and k_2 = 0.25 and two input frequencies. (c) Stability analysis. Real part of the dominant poles versus k_1. (d) Injection-locked curve versus k_1 for k_2 = 0.25 and E_g = 0.63 V.

III. Semi-Analytical Study

The goal will be to investigate the impact of the coupled network, depending on k_1 and k_2, on the locked behavior. Thus, the observation node will be the one at which the coupled inductor L_1 is connected. We will describe the oscillator core with a nonlinear admittance function Y, extracted with the aid of a voltage AG [8], introduced in parallel at the L_1 node [Fig. 1(c)]. The extraction is carried out in HB (with NH harmonic terms), in the presence of the input source, with a given amplitude E_g and frequency ω. We perform a double sweep in the AG phase ϕ and amplitude V and calculate the admittance function $Y(V,\phi,\omega)$ as the ratio between the AG current and voltage. Assuming periodic operation at ω and applying Kirchoff's laws at the analysis node, we obtain:

$$Y(V,\phi,\omega)+j/(L_1\omega)+Y_c(k_1,k_2,\omega)=0 \qquad (3)$$

where Y_c is the admittance exhibited by the coupled network (Fig. 1). Note that $Y(V,\phi,\omega)$ was extracted in the presence of L_1, so it is necessary to subtract the L_1 admittance from Y. Though Y is extracted with NH harmonics, the coupling to the external resonators is considered at ω only. This is a reasonably approximation due to the filtering effects of the oscillator output. Note that the phase ϕ of the solutions of (3) should ideally agree with the phase of $Z_{AG}(I_{AG},\omega,k_1,k_2)/F_{th}(\omega)$ in

(1). We will make use of the conventional assumption of identical resonance frequencies of the two external resonators [5], agreeing with the input frequency: $1/\sqrt{L_2C_2}=1/\sqrt{L_3C_3}=\omega$. In these conditions, Y_c becomes:

$$Y_c(k_1,k_2)=\frac{R_{p2}R_L+k_2^{\,2}L_2L_3\omega^2}{jL_1\omega\left(R_{p2}R_L+k_2^{\,2}L_2L_3\omega^2\right)+k_1^{\,2}L_1L_2\omega^2R_L} \quad (4)$$

where R_{p2} is the loss resistance in the intermediate resonator. Note that the loss resistance of L_1 (R_{p1}) can be introduced in Y and that of L_3 (R_{p3}) can be absorbed in R_L. However, for the moment we will assume $R_{p1}=R_{p3}=0$ since their effect will be analyzed in detail later in this section. As gathered from (4), R_{p2} will have a higher impact for a smaller k_2. Thus, we will avoid too small values of k_2, with no limitation in k_1. In these conditions, we may neglect R_{p2}, which leads to:

$$Y_c(k_1,k_2)=\frac{Q_3^{-1}(k_1/k_2)^2-j}{L_1\omega\left[1+Q_3^{-2}\left(k_1/k_2\right)^4\right]} \quad (5)$$

where $Q_3^{-1}=\omega C_3R_L$. The ratio $x=k_1^{\,2}/k_2^{\,2}$ and Q_3^{-1} can be compacted in a single parameter $r_q=Q_3^{-1}x$, which provides:

$$Y_c(r_q)=\frac{r_q-j}{L_1\omega\left(1+r_q^{\,2}\right)} \quad (6)$$

Replacing the above expression in (3) and splitting into real and imaginary parts, we obtain:

$$\begin{aligned}H^r(V,\phi,r_q)&=Y^r(V,\phi)+\frac{r_q}{L_1\omega\left(1+r_q^{\,2}\right)}=0\\ H^i(V,\phi,r_q)&=Y^i(V,\phi)+\frac{1}{L_1\omega}-\frac{1}{L_1\omega\left(1+r_q^{\,2}\right)}=0\end{aligned} \quad (7)$$

where the superscripts r and i indicate real and imaginary parts. As observed in (7) the locked solutions only depend on $Y(V,\phi,\omega)$ and the parameter r_q. For $r_q=0$ we have $k_1=0$, so the external resonators become uncoupled from the oscillator. Thus, system (7) particularizes to $Y(V,\phi,\omega)=0$, which provides the periodic solutions of the standalone locked oscillator. For each r_q, the solutions of (7) are given by the intersections of the two zero-value contours $H^r(V,\phi,r_q)=0$ and $H^i(V,\phi,r_q)=0$ in the plane defined by V and ϕ, calculated in in-house software. The output power P_{out} and drain efficiency E_{eff} vary versus r_q as shown in Fig. 3. There is a narrow r_q interval for which (7) only has a low-amplitude solution and the system is unlocked. The maximum output power and efficiency are obtained in the curve C2, existing for a larger r_q interval. Note that the drain efficiency is quite high, owing to the near-ideal MOSFET switching. The k_1 and k_2 leading to a same pair of values $P_{out}(r_q)$, $E_{eff}(r_q)$ are related as:

$$k_1=\frac{r_q}{\sqrt{R_L}\sqrt{\omega C_3}}k_2 \quad (8)$$

If we wish to obtain $P_{out}(r_q)$, $E_{eff}(r_q)$ for a smaller k_1 (larger distance d_1 between the oscillator and first resonator), we should increase R_L. This is convenient since it reduces the impact of R_{p2} [see (4)]. The predictions of (7) have been validated with HB considering five values of r_q (indicated in Fig. 3) and three R_L values for each r_q, given by $R_L=25\ \Omega$, $50\ \Omega$, $100\ \Omega$. Note that each R_L is associated to a ratio k_1/k_2 through the relationship (8). As seen in Fig. 3, under a same choice of r_q, we obtain the same values of output power and efficiency (overlapped HB points). As an additional validation, we have expressed k_1 as in (8) and performed a sweep of k_2, under a constant $r_q=0.456$, which provides $P_{out}=1.2$ W. We have also considered $R_L=50\ \Omega$ and three values of the loss resistance $R_{p2}=0\ \Omega$, $1\ \Omega$ and $2\ \Omega$. In the lossless case, P_{out} keeps constant for all k_2. When considering losses, P_{out} decreases with R_{p2} in the lower k_2 interval, as predicted by (4). For $k_2>0.15$, the impact of R_{p2} is negligible.

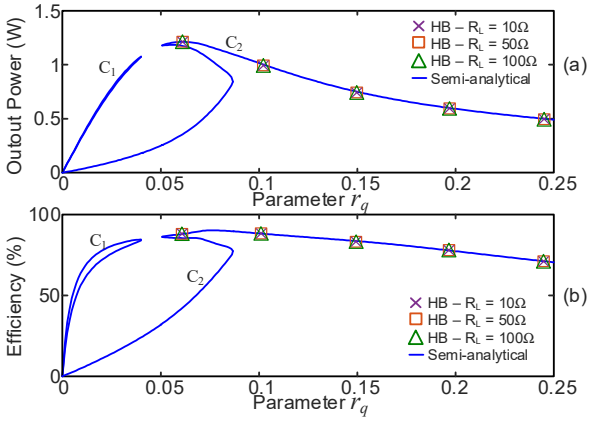

Fig. 3. Solution curves of the injection-locked oscillator obtained by solving (7) versus r_q. Validation with independent HB for five r_q values and three load resistance $R_L=25\ \Omega$, $50\ \Omega$, $100\ \Omega$ for each r_q. (a) Output power. (b) Efficiency.

Next, we will analyze the impact of the loss resistances R_{p1} and R_{p3}. We will assume $k_2=0.2$ (in the order of previous works [11]), so the impact of R_{p2} will initially be neglected. As easily derived, in the presence of R_{p1}, the total impedance in series with C_1 [Fig. 1(a)] is $Z_T^r=R_{p1}+R_L'(k_1/k_2)^2$, where $R_L'=R_L+R_{p3}$. Thus, for a given k_2, the power delivered to R_L' will increase with k_1^2 and R_L' For $k_2=0.2$ and $R_L'=52\ \Omega$, the power delivered to the coupled network will be dominant provided that $k_1>0.04$. To calculate the output power, we can use the same function $Y(V,\phi,\omega)$ and introduce R_{p1} and R_{p3} in Y_c:

$$Y_c\left(k_1,k_2,R_{p1},R_{p2}\right)=\frac{Y_c^{\,r}(r_q')+R_{p1}\left|Y_c(r_q')\right|^2+jY_c^{\,i}(r_q')}{1+2Y_c^{\,r}(r_q')R_{p1}+R_{p1}^{\,2}\left|Y_c(r_q')\right|^2} \quad (9)$$

where $Y_c(r_q')$ is the admittance in (6), evaluated at $r_q'=\omega C_3R_L'x$. The output power is given by:

$$P_{out}=\frac{R_L}{R_L+R_{p3}}\frac{1}{2}Y_c^{\,r}\left(k_1,k_2,R_{p1},R_{p2}\right)V^2 \quad (10)$$

where V is obtained from (3), after introducing (9). The above results have been verified with full HB, considering $R_{p1}=R_{p2}=R_{p3}=2\ \Omega$ (Fig. 4) and the three load resistances $R_L=25\ \Omega$, $50\ \Omega$, $100\ \Omega$ (Fig. 5). Even in the presence of losses, the maximum (marked with a black circle) shifts to lower k_1 as R_L increases, in agreement with the analytical predictions.

The circuit has been experimentally characterized with the setup of Fig. 6(a), by means of a high-impedance probe connected to a Digital Sampling Oscilloscope DSO6034A. The

coils are implemented with AWG18 copper wound on machined acrylic sheets to provide the approximate inductance L = 2.68 µH. The variation of the coupling factor with the distance has been determined from the measurement of the scattering parameters [11]. Fig. 6(b) presents the voltage waveform at $R_L = 100\ \Omega$, obtained at the total distance $d_1+d_2 = 13$ cm. Measurements are superimposed in Fig. 5, with very good qualitative agreement. Discrepancies are due to inaccuracies/tolerances in the component models, as well as the limitations of the lumped equivalent model of the coupled coils. in the models of the active device and coupled coils. We have achieved an efficiency of 80% at 13 cm, which significantly exceeds the one in [9].

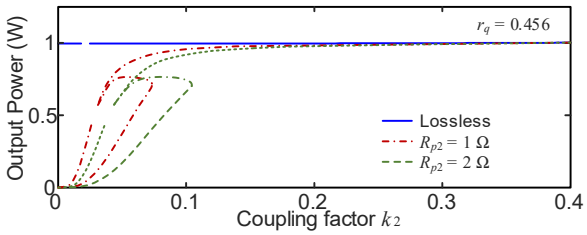

Fig. 4. Solution curves versus k_2 when expressing k_1 as in (8), under $r_q = 0.456$, $R_L = 50\ \Omega$ and three values of the loss resistance: $R_{p2} = 0\ \Omega$, 1 Ω and 2 Ω.

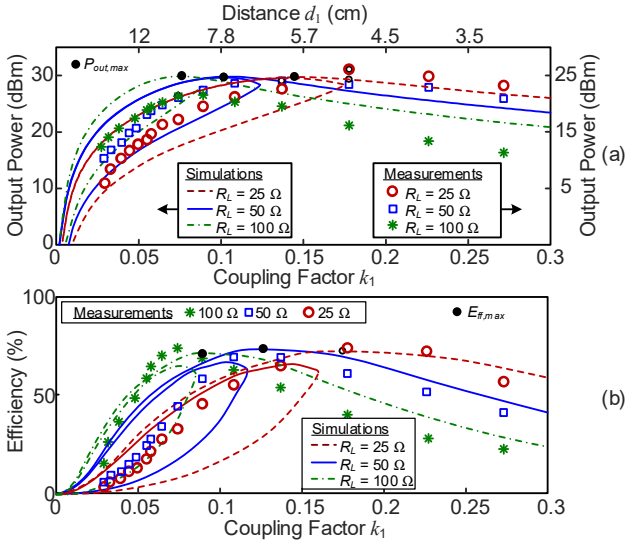

Fig. 5. Injection-locked oscillator analyzed with the full HB method of Section II. Experimental points superimposed. As R_L increases the output power maximum shifts to lower k_1. (a) Output power. (b) Efficiency.

IV. Conclusion

The behavior of an injection-locked oscillator coupled to two external resonators has been investigated. We have derived a semi-analytical formulation, which, under negligible losses in the intermediate resonator, provides the solutions of the locked oscillator in terms of a single non-dimensional parameter. The formulation, validated with HB and measurements, enables an insightful understanding of the solution dependence on the coupling factors and load and parasitic resistances.

Acknowledgment

Work supported by MCIN/AEI/10.13039/501100011033, (grant PID2020-116569RB-C31) and by the Consejería de Universidades, Igualdad, Cultura y Deporte del Gobierno de Cantabria (Contrato Programa Gobierno de Cantabria – UC).

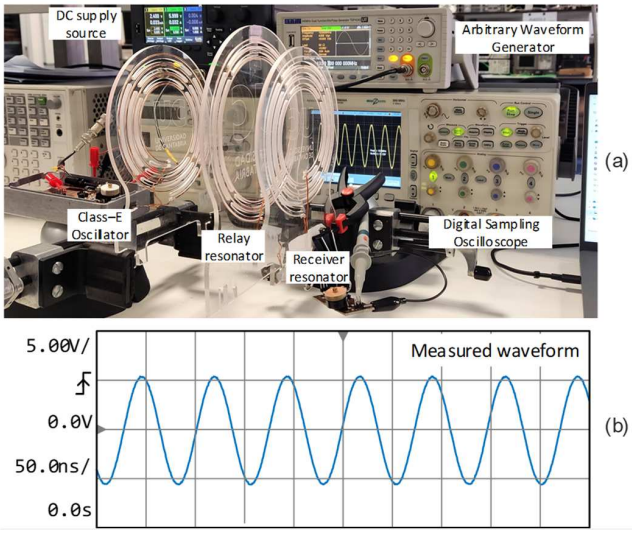

Fig. 6. Experimental characterization. (a) Measurement setup. (a) Voltage waveform at $R_L = 100\ \Omega$, obtained for the total distance $d_1+d_2 = 13$ cm.

References

[1] G. Monti, G. De Giovanni, M. De Liso, M. Pascali, and L. Tarricone, "Wireless Power Transfer Strategies for Medical Implants: Focus on Robustness and EM Compatibility," *IEEE Microwave Magazine*, vol. 22, no. 9, pp. 28–41, Sept. 2021.

[2] D. M. Roberts, A. P. Clements, R. McDonald, J. S. Bobowski and T. Johnson, "Mid-Range Wireless Power Transfer at 100 MHz Using Magnetically Coupled Loop-Gap Resonators," *IEEE Trans. Microw. Theory Tech*, vol. 69, no. 7, pp. 3510–3527, July 2021.

[3] X. Liu, X. Song, X. Yuan, "Compensation Optimization of the Relay Coil in a Strong Coupled Coaxial Three-Coil Wireless Power Transfer System," *IEEE Trans. Power Electronics*, vol. 37, no. 4, pp. 4890–4902, April 2022.

[4] M. Machnoor, E. S. Gámez Rodríguez, P. Kosta, J. Stang, G. Lazzi, "Analysis and Design of a 3-Coil Wireless Power Transmission System for Biomedical Applications," *IEEE Trans. on Antennas and Propagation*, vol. 67, no. 8, pp. 5012–5024, Aug. 2019.

[5] B. Zhang and S. Lam, "Gate-Driverless Wireless Power Transfer Circuits: a Gallium-Nitride (GaN) Colpitts Oscillator Compared with Its Silicon Counterpart," *2022 IEEE Asia Pacific Conference on Postgraduate Research in Microelectronics and Electronic*, Shenzhen, China, 2022.

[6] V. Ardila, F. Ramirez, and A. Suarez, "Nonlinear Dynamics of an Oscillator Inductively Coupled to an External Resonator for Power Transfer and Data Transmission," *IEEE Trans. Microw. Theory Tech.*, vol. 70, no. 4, pp. 2418–2431, Apr. 2022.

[7] V. Ardila, F. Ramírez and A. Suárez, "Analysis of an Oscillatory System With Three Coupled Coils for Wireless Power Transfer," *IEEE Trans. Microw. Theory Tech.* DOI: 10.1109/TMTT.2023.3330366.

[8] V. Ardila, F. Ramirez and A. Suárez, "Analysis and Design of Injection-Locked Oscillators Coupled to an External Resonator," *IEEE Trans. Microw. Theory Tech*, vol. 71, no. 10, pp. 4546–4561, Oct. 2023.

[9] K. Lee and S. H. Chae, "Power Transfer Efficiency Analysis of Intermediate-Resonator for Wireless Power Transfer," *IEEE Trans. on Power Electronics*, vol. 33, no. 3, pp. 2484–2493, March 2018.

[10] J. M. Collantes, I. Lizarraga, A. Anakabe, and J. Jugo, "Stability verification of microwave circuits through Floquet multiplier analysis", in *Proc. IEEE Asia-Pacific Circuits Syst.*, 2004, pp. 997–1000.

[11] J. J. Kim, J. Kim, "Modeling method of coil module for wireless power transfer system by two-port S-parameter measurement in frequency domain," *2014 IEEE Wireless Power Transf. Conf.*, Jeju, Korea (South), pp. 251–254.